

pubs.acs.org/acscatalysis Viewpoint

# Toward Intrinsic Catalytic Rates and Selectivities of Zeolites in the Presence of Limiting Diffusion and Deactivation

Cole W. Hullfish,<sup>‡</sup> Jun Zhi Tan,<sup>‡</sup> Hayat I. Adawi,<sup>‡</sup> and Michele L. Sarazen\*



Cite This: ACS Catal. 2023, 13, 13140-13150



**ACCESS** |

III Metrics & More

Article Recommendations

#### 1. INTRODUCTION

The goal of atom- and energy-efficient production of fuels and chemicals from renewable (i.e., biomass) and closed-carbon (i.e., CO<sub>2</sub> and waste plastic) feedstocks requires effective catalysts. In order to design effective catalysts that utilize all active sites to their fullest extents, increase selectivity to desired reaction pathways, and remain stable for multiple life cycles, a molecular understanding of their performance is needed. However, many of our target conversions involve complex reaction networks where communication between active sites in a given catalyst affects measured rates and selectivities, thus obfuscating interpretation of intrinsic kinetics. When these sites are in microporous environments, such as zeolites and certain metal-organic frameworks (MOFs), the initial ingress into a crystal or diffusion between sites becomes even more relevant because effective diffusivities decrease as molecule sizes approach that of confining voids. Further, diffusionenhanced secondary reactions can shift measured product selectivities away from those intrinsically governed by the active site. Apparent selectivities consequently skew toward reactions that form products with relatively low egress barriers (e.g., through isomerization). This selection sometimes mitigates deactivation, but deactivation can also be exacerbated during diffusion-limited hydrocarbon conversions due to active site blockage or pore occlusion by carbonaceous foulants. Thus, rigorous deconvolution of reaction-diffusion-deactivation phenomena is vital for the extraction of intrinsic rates and selectivities that will support next-generation catalyst design.

One catalyst design strategy to overcome said limitations is the introduction of auxiliary porosity to increase effective diffusivities of reactant and product species. For example, mesopores may be introduced through direct synthesis or postsynthetic modification of microporous supports. 1-4 Since selectivities within diffusion-limited reaction systems depend on the ease of product egress and formation of bulky transition states, introduction of secondary mesoporosity can increase turnovers due to enhanced diffusion and impact product distributions due to reduced intracrystalline residence times (which mitigate secondary reactions). Mesopores also influence deactivation by coking because relative coke accumulations in micropores or mesopores affect both active site density and diffusion. 5-10 These consequences can make treatments of reaction-diffusion-deactivation phenomena in (hierarchical) zeolites challenging but can also extend the catalyst lifetimes and prolong micropore catalysis when coke deposition is redistributed to mesopores.

In this Viewpoint, we discuss how fundamental insights are gained from deconvolution of reaction—diffusion—deactivation in four different examples of hydrocarbon reactions on zeolites. We first explore how hydrocarbon chain growth during alkene oligomerization competes with secondary  $\beta$ -scission to decrease and increase product diffusivities, respectively. These competing effects on diffusivity as a function of reaction progress have significant implications on reactivity and selectivity as the zeolite pore size and connectivity change. Second, we highlight hierarchical (microporous-mesoporous) zeolites, which mitigate the cooperativity of reactiondiffusion-deactivation by increasing catalytic efficiency of protons and delaying kinetic manifestations of deactivation (i.e., dampened apparent rate constants). To grapple with the wide synthetic scope of hierarchical zeolites, we delineate a straightforward reaction-diffusion analysis scheme to determine whether selected (post)synthetic mesopore incorporation methods sufficiently enable kinetic control of reaction systems that are otherwise prohibitively diffusion-limited in micropores. This was done using a simple "complex" reaction family: parallel etherification and alkylation reactions of benzyl alcohol with itself or with trimethylbenzene, respectively, which have diffusivities that vary enough to become kinetically relevant probes in microporous materials. Third, we stress the diffusion complications on ingress of exceptionally large polymeric reactants that seemingly cannot enter zeolite micropores at initial time points. Proper deconvolution of measured performance into meaningful metrics of intrinsic rates and selectivities to compare across studies is challenging. In this case, the normalization of reactant consumed, or products produced, by total (or surface) active site density and reaction time can serve as a primitive metric for catalytic rate comparison between zeolites with different framework structures and acid site densities. The final example extends these reaction-diffusion-deactivation phenomena to bifunctional catalytic systems, as the addition of metal functions to



zeolites can enable unique reactivities and mitigate coking due to the orthogonal metal catalysis. These effects are rooted in acid—metal diffusion that generates varied concentration gradients of chemical species relative to the isolated acid catalysis; therefore, proximity of acid and metal functions is a critical consideration for kinetics and deactivation, especially in diffusion-limited regimes.

### 2. THE CASE FOR INTRINSIC KINETICS: ALKENE OLIGOMERIZATION AS A MODEL REACTION

Light alkene (i.e., propene) oligomerization acts as an interesting case study of a small reactant that undergoes subsequent conversions into products that are increasingly diffusion-constrained. Consequently, measured reactivities and selectivities are extremely sensitive to the sizes of the environments surrounding protons in aluminosilicates (zeolites and mesoporous acids) due to contributions of both confinement and diffusion. Alkene conversion on solid acids involves concurrent oligomerization, isomerization,  $\beta$ -scission, hydride transfer, and cyclization that yield a complex product pool of various carbon chain lengths, structures (e.g., branching or rings), and saturation. 11-15 Rapid skeletal and double-bond isomerizations give isomers different from those initially formed via oligomerization events, requiring assessment of pools of equilibrated species. The relative rates of these different reactions are influenced by channel sizes in microporous solid acids, which sieve reactants, control product egress, and selectively accommodate formation of transition states based on their sizes and conformations. 16,17 Onedimensional zeolites (TON, MOR) and mesoporous acids, such as Al-MCM-41, amorphous silica-alumina (SiAl), and silica-supported polyoxometalates (POM), are shown to preserve the chain length of oligomerization products (true oligomers). 18-20 Their lack of tortuosity allows for unobstructed diffusion of carbon chains formed within their channels and voids.<sup>21</sup> In contrast, materials with undulating pore diameters created by channel intersections (MFI, BEA) or cage-window frameworks (FAU) result in the local formation of oligomers larger than the intervening passages. This change in environment required  $\beta$ -scission events for the facile egress of products (Figure 1).

Extracted rate constants on this same series of zeolites increase with decreasing zeolite void diameter, consistent with more favorable van der Waals solvation of the bimolecular dimerization transition states than of the monomolecular alkene-derived precursors.<sup>18</sup> Within a given zeolite framework (here, MFI), propene dimerization rates decrease with initial time-on-stream before reaching a steady state rate.<sup>22</sup> Further, rates decrease with increasing crystallite size on samples with low proton density, suggesting that intrazeolite transport limitations influenced measured rates. In fact, rate reductions increase in severity under reaction conditions that favor the formation of heavier products and are further plagued by transient changes in rates upon step-changes in reaction temperature or reactant pressure.<sup>22</sup> Using effectiveness factor formalisms to extract the product of the effective rate constant and diffusivity, it is shown that not only are selectivities governed by diffusion as discussed above but oligomerization rates are as well. The composition of hydrocarbon products that accumulate within zeolite micropores during alkene oligomerization alters effective diffusivities: lower propene pressures result in pores filled with lower molecular weight products and higher resultant effective diffusivity, while higher

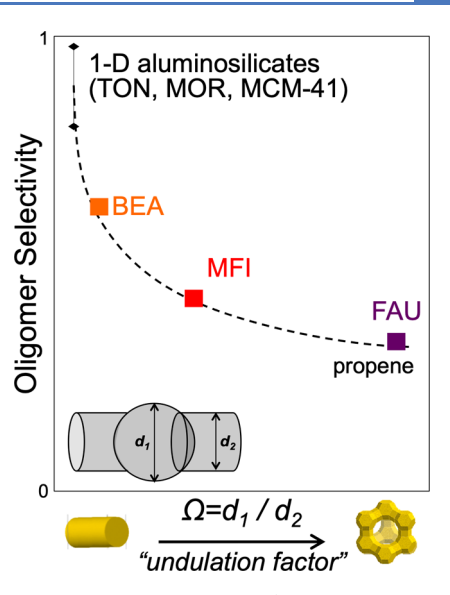


Figure 1. Selectivity to true oligomers (i.e., not β-scission products) as a function of the diffusion pathway in aluminosilicates. The undulation factor is defined as the ratio of the largest cavity to pore-limiting diameters and captures the extent of undulations in the zeolite void system. Adapted from ref 21. Copyright 2016 American Chemical Society.

propene pressures result in pools of trimers, etc. that significantly decrease extracted diffusivity values. However, when properly accounting for the reduction in the effective diffusivity of propene and product alkenes with increasing propene pressure, the increasingly negative-order dependence on propene pressure with decreasing proton density can be reconciled with these results as well as previous reports. These studies on alkene oligomerization highlight a case when one may have initial deactivation but reach a steady state once the pores become filled, so that only diffusion impacts measured rates and selectivities.

## 3. DECOUPLING INTRINSIC REACTIVITY FROM DIFFUSION AND DEACTIVATION IN (HIERARCHICAL) ZEOLITES

Reaction and diffusion also interplay with deactivation to varying extents.  $^{24-26}$  Their cooperativity intensifies in diffusion-constrained reactions on zeolites, thus motivating the use of modified hierarchical zeolites with auxiliary mesoporous (2-50 nm) voids to alleviate transport barriers. <sup>25,27-29</sup> Reported increases in conversions (of limiting reactants at specific reaction times or total turnovers), catalytic lifetimes, and selectivities to bulky products in hierarchical zeolites compel rigorous investigation into the intrinsic kinetics underlying those observations. 30-32 We have expanded upon initial Thiele modulus analyses of hierarchical performance in different reactions, 21,33-36 by rigorously evaluating reactiondiffusion-deactivation during the competing, liquid-phase reactions of benzyl alcohol (BA) with 1,3,5-trimethylbenzene (TMB) or itself to respectively yield 1,3,5-trimethyl-2benzylbenzene (TM2B) or dibenzyl ether (DBE). These probes exclusively interrogated how molecular sterics in confining environments impacted diffusion and observed activity, as the parallel reactions have different sensitivities to diffusion constraints. Our work considered a comprehensive suite of (hierarchical) zeolites varying in crystal size, mesoporosity, proton density, and parent architecture. 27,3

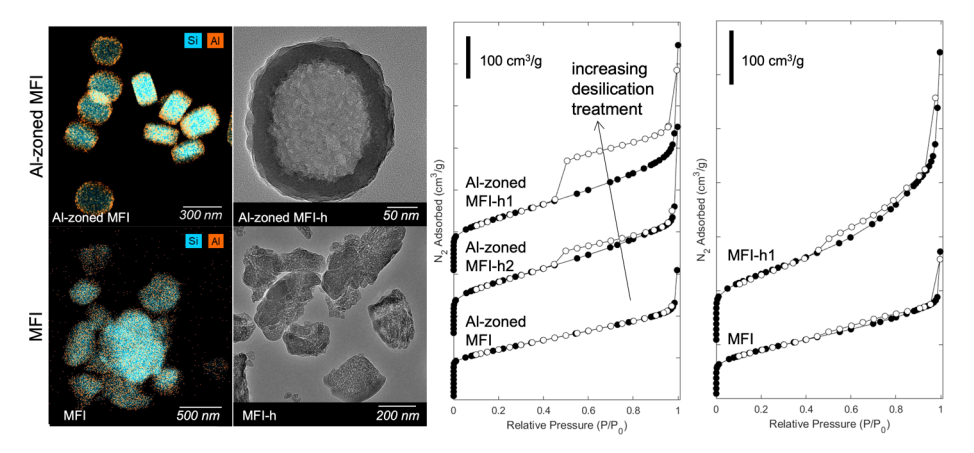


Figure 2. (Left) STEM-EDXS and TEM of Al-zoned and Al-uniform MFI. (Right) N<sub>2</sub> physisorption isotherms of hierarchical analogues (MFI-h) synthesized from Al-zoned and Al-uniform MFI using desilication in NaOH. Adapted from ref 37. Copyright 2023 American Chemical Society.

We contextualized the intrinsic reactivities and propensities for deactivation of hierarchical zeolites during reactions of (poly)substituted aromatics according to baseline diffusion barriers imposed by microporous zeolite crystal sizes and pore architectures.

When Thiele moduli  $(\phi)$  are high  $(\phi \gg 1)$ , rate constants fitted to experimental reaction data reflect apparent diffusion barriers; thus, this analysis requires assessment of  $\phi$ .<sup>38</sup> The intrinsic rate constant for first-order reaction of species i  $(k_{i,int})$  in a spherical catalyst pellet can be derived from reaction—diffusion treatment of its apparent analogue  $(k_{i,app})$ .<sup>27,39</sup> The associated derivation is mediated by the assumption that the effectiveness factor  $(\eta)$  simplifies to  $\eta = 1/\phi$  under severe diffusion constraints:

$$\phi = \frac{R}{3} \left[ \frac{k_{i,\text{int}} \rho_{H+}}{D_{e,i}} \right]^{1/2}$$
(1a)

$$\phi = \frac{1}{\eta} = \frac{k_{i,\text{int}}}{k_{i,\text{app}}} \tag{1b}$$

$$\frac{k_{i,\text{int}}}{k_{i,\text{app}}} = \frac{R}{3} \left[ \frac{k_{i,\text{int}} \rho_{H+}}{D_{e,i}} \right]^{1/2}$$
(1c)

$$k_{i,\text{int}} = \frac{\rho_{H+} R^2}{D_{e,i}} \left[ \frac{k_{i,\text{app}}}{3} \right]^2$$
 (1d)

Here, R is the spherical catalyst crystal radius,  $D_{e,i}$  is the effective diffusivity of species i, and  $\rho_{\rm H+}$  is the volumetric catalyst proton density. Similar reaction-diffusion treatments were previously utilized for methylcyclohexane ring contraction on Keggin-type polyoxometalates supported on mesoporous silica and physically mixed with Pt on alumina.<sup>38</sup> Such treatments rely on measured or calculated effective diffusivities within a specified zeolite architecture, which has structural periodicity that facilitates computational estimates of Dei (as from density functional theory or molecular dynamics).44 Dei may also be deduced experimentally through pulsed-field gradient NMR, sorption rate measurements, or chromatographic methods. 43 It is worth emphasizing that these  $D_{e,i}$  are averaged transport parameters accounting for complex zeolitic channel networks that vary in void diameters and tortuosity.<sup>44</sup> Moreover, measurements do not give  $D_{e,i}$  absolutely but are

scaled as  $D_{e,i}/L^2$ , where L is the characteristic length of the sample that can be obfuscated from microscopy techniques if crystal aggregates are present.<sup>39,45</sup> The baseline  $k_{i,int}$  for microporous architectures yields insight into subsequent mesopore effects on rates in hierarchical zeolites. However, fewer estimates of  $D_{e,i}$  are tabulated for hierarchical zeolites because their synthetic space is vast and actively growing. For hierarchical zeolites, available  $D_{e,i}$  are averages across extensive heterogeneities in (meso)pore distributions. Core-shell hierarchical zeolites offer the most extreme example<sup>37</sup> because stark separation of microporous and mesoporous phases leads to two distinct diffusion regimes. For example, we previously demonstrated that core-shell mesoporosity resulted from desilication of MFI zeolites having shells (within 20 nm of crystallite surfaces) with high Al density (Si/Al < 25), which prevented cleavage of Si-O-Si bonds by NaOH (Figure 2). In contrast, low Al density in MFI cores (Si/Al > 50) enabled significant dissolution of internal Si-O-Si. Increasing desorption hystereses with desilication time in N2 physisorption isotherms reflected increasing volumes of occluded mesopores without direct access to crystallite surfaces. Such hystereses were absent for MFI-h prepared by desilication of MFI with uniform Al density within the optimal desilication range (Si/Al = 40). The notable difference in mesopore distribution, despite use of identical desilication parameters (0.2 M NaOH, 338 K, 30 min), manifested in different diffusion regimes for reaction moieties that preceded coke formation, consistent with different weight percent coke accumulation on each MFI-h (relative to dry catalyst masses) after 2 h of reaction.<sup>37</sup> Mesopore zoning has similarly been achieved with surfactant-mediated formation of core-shell structures with occluded mesopores as opposed to ones open to the external crystal surface. 46 Clearly, any estimated  $D_{ei}$ exclusively describes diffusion through one hierarchical zeolite derived from one postsynthetic treatment applied to one parent zeolite. Therefore, the physical implications of individual  $D_{e,i}$ measurements are rendered insignificant in the face of propagating variations of mesopore synthesis treatments, and methods of estimating impact are needed.

As with  $D_{\mathrm{e},\nu}$  the  $k_{i,\mathrm{app}}$  for hierarchical zeolites reflects a net apparent reaction rate constant for protons located in micropores and mesopores (if both exist), which would result in different transition state confinement and thus activation energies. In hierarchical zeolites prepared via postsynthetic desilication,  $k_{i,\mathrm{app}}$  primarily reflects microporous confinement

ACS Catalysis pubs.acs.org/acscatalysis Viewpoint

because desilication terminates mesopore surfaces with silanol groups. Thence, mesopore-confined protons only exist in desilicated zeolites where the desilication front terminates at the mouth of a microporous void, so that micropore protons are directly accessible from the proximal mesopore. When hierarchical zeolites are instead prepared via hydrothermal mesopore templating, a significant portion of protons are located at mesopore surfaces and impact the net  $k_{i,\mathrm{app}}$  according to their proportion of the total proton density. Application of eqs 1a–1d to the net  $k_{i,\mathrm{app}}$  therefore will yield a  $k_{i,\mathrm{int}}$  proportional to the net mesopore-weighted activation energy.

Using the probe alkylation of TMB with BA on a set of 15 synthetically diverse (hierarchical) zeolites, we demonstrated that limitations on  $D_{\rm e,i}$  measurements for reaction—diffusion analysis are overcome by estimating diffusivity thresholds required for kinetically controlled catalysis from eq 1a (with  $\phi=1$ ).  $D_{\rm e,i}$  is then back-calculated for a first-order reaction in a spherical zeolite crystal from easily measured values (Figure 3):

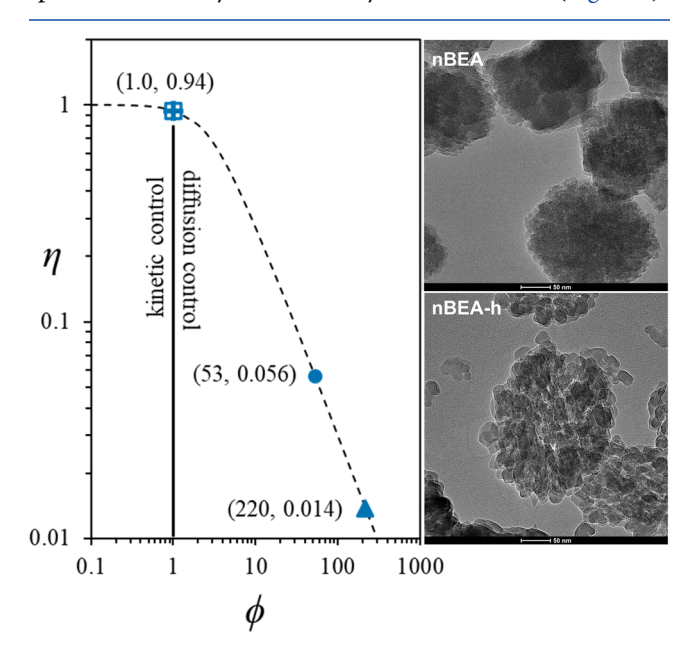


**Figure 3.** Effectiveness factor as a function of the Thiele modulus for nBEA ( $\bullet$ ),  $\mu$ BEA ( $\blacktriangle$ ), nBEA-h ( $\square$ ), and  $\mu$ BEA-h (+) showing shift to  $\phi = 1.0$  at the threshold of kinetic control. Reproduced from ref 27. Copyright 2021 Royal Society of Chemistry.

R from (S)TEM or SEM;  $k_{\rm i,app}$  from fitted rate data; and  $\rho_{\rm H+}$  measured from titration by NH<sub>3</sub>, propylamine, or pyridine. Back-calculated  $D_{\rm e,i}$  for species i in hierarchical zeolites are then contrasted against reported  $D_{\rm e,i}$  within their microporous parents to determine whether the necessary increases in diffusivity of i required for  $\phi=1.0$  are feasible (i.e., within 2 orders of magnitude) for the hierarchical case. This above analysis of eq 1a when  $\phi=1$  requires one value from the literature or measured experimentally: the  $D_{\rm e,i}$  for mass transport of species i in the microporous parent of the studied hierarchical zeolite at the studied reaction temperature. All other parameters  $(R, \rho_{\rm H+}, {\rm and}\ k_{\rm i,app})$  for the hierarchical zeolite are obtained experimentally.

For TMB alkylation, parent MOR and hierarchical MOR (MOR-h) of varying crystal diameter scales (nanocrystalline (n) with  $d_{\rm crystal}$  < 200 nm or microcrystalline ( $\mu$ ) with  $d_{\rm crystal}$  > 500 nm) were prepared through identical postsynthetic

treatments. This feasibility study showed that the large crystal radius of microcrystalline MOR (µMOR), which maintained the same nominal crystal radius after postsynthetic treatments, oversaturated eq 1a, leading to an unrealistically high threshold  $D_{e,i}$  for its  $\mu$ MOR-h analogue. Consequently, the postsynthetic treatment that effectively yielded kinetically controlled catalysis for nMOR-h was unable to similarly mitigate diffusion control in  $\mu$ MOR-h due to its large crystallite size ( $d_{crystal} \sim 20 \ \mu m$ ) and resistance to selected leaching treatments due to lower Si/ Al than nMOR (Si/Al = 7.7 and 10, respectively). Kinetically controlled catalysis is hence only feasible in hierarchical zeolites to the extent that  $D_{e,i}$  enhancements compensate for initial reaction-diffusion setbacks owing to large crystal size. Therefore, we recommend the analytical scheme of equating eq 1a to unity to guide, inform, and contextualize new (applications of) mesopore incorporation methods and their potentials to successfully mediate kinetic control.

As  $\phi$  scales with  $L^2/D_{\mathrm{e},\nu}$  increased mesoporosity and reduced crystallite size can separately and synergistically minimize  $\phi$ . Commercially, low  $\phi$  has been achieved predominantly using zeolite nanocrystals with L < 200 nm.<sup>37</sup> Small crystallites delay complete fouling by reducing the number of protons accessed by molecules traversing the micropore network before crystal egress, thus minimizing the number of undesired secondary turnovers that would otherwise form bulky coke molecules. However, as kinetic diameters of diffusing reactants approach or exceed the porelimiting diameters of micropores, the increased energy barriers for activated diffusion inflate  $\phi$  and increase coking rates due to higher molecule residence times. Thus, the commercial feasibility of zeolites for reactions converting or producing bulky molecules necessitates incorporation of mesopores to alleviate deactivation phenomena.

We broadly define kinetically relevant deactivation as deactivation that causes apparent and/or intrinsic reaction rates to irreversibly decrease and (potential) selectivities to change.<sup>48</sup> Kinetically relevant deactivation reduces site (here, proton) densities via poisoning and/or pore occlusion, thereby damping apparent reaction rates with time-on-stream or clock time. In batch systems, deactivation causes reaction rates to decrease faster than is otherwise typically expected as reactants are consumed. However, deactivation may also impact intrinsic (hierarchical) zeolite reactivities by altering energies of transition state confinement because deposition of carbonaceous species changes effective void diameters. These phenomena require a mathematical assessment of at least the former, more straightforward activity losses through use of empirical activity decay rate laws that model temporal losses of proton density. These decay rates  $(r_D)$  are typically derived as separable from reaction rates:<sup>49</sup>

$$r_{\rm D} = -\frac{\mathrm{d}a}{\mathrm{d}t} = g[a(t)]k_{\rm D}f([\mathrm{Reactants}], ..., [\mathrm{Products}]) \tag{2}$$

Here,  $k_{\rm D}$  is the deactivation rate constant at a specific temperature, g[a(t)] is the functional form of activity in decay, and  $f([{\rm Reactants}],...,[{\rm Products}])$  is a function of any reaction moieties that mediate deactivation. Some functional forms better describe specific deactivation mechanisms. For example, sintering is commonly described with second-order activity decay with f=1:

$$r_{\rm D} = -\frac{\mathrm{d}a}{\mathrm{d}t} = k_{\rm D}a^2 \tag{3}$$

For the diffusion-constrained reaction systems of interest to this Viewpoint, coking prevails as the primary deactivation phenomenon and is most often described by empirical decay laws. In these cases, specifications of f require hypothesized, reported, or experimentally deduced mechanisms for coke formation from identified coke precursors. For probe TMB alkylation, we demonstrated that first-order activity decay reasonably estimated temporal proton losses.<sup>27</sup> Higher coke accumulations at equivalent reaction times (120 min) corresponded to higher  $k_{\rm D}$  values for microporous zeolites of varying crystal size. In contrast, hierarchical zeolites (i.e., nMFI-h) typically accumulated more coke within 120 min while giving significantly lower  $k_{\rm D}$  than their microporous parents (i.e., nMFI).<sup>37</sup> We hence deduced that hierarchical zeolites can accumulate more foulants before exhibiting measurable deactivation kinetics. The preferential location of coke deposition in hierarchical zeolites remains under active investigation and depends on the location of protons and the connectivity of each mesopore to micropores, other mesopores, and the zeolite crystal surface. 8,50,51 This connectivity in turn depends on the method of mesopore incorporation, as hydrothermal templating methods may yield less mesoporemesopore and mesopore-surface connectivity than postsynthetic leaching methods.<sup>52</sup>

The decay rate laws described here enable crucial deconvolution of reaction and deactivation kinetics. We emphasize that this deconvolution is necessary to ensure that fitted apparent reaction rate constants are correctly normalized by (reduced) proton densities under deactivating conditions. In turn, accurately normalized apparent rate constants will give accurate diffusion-corrected intrinsic rate constants when the recommended diffusion corrections (eqs 1a-1d) are applied.

## 4. THE PURSUIT OF REACTION RATES FOR EXCESSIVELY LARGE REACTANTS ON MICROPOROUS ZEOLITES

While the probe aromatic alkylation network described in Section 3 can examine potential diffusion limitations in some zeolites, even larger reactants like polymers in waste plastic upcycling further engender assessment of reactant size accessibility in different pore environments. Hydroconversion, particularly catalytic cracking in the presence of H<sub>2</sub> on metalloaded zeolites, is interesting due to higher selectivity toward saturated hydrocarbons and lower operating temperatures compared to catalytic cracking or pyrolysis under N2. The impact of hydrocarbon chain length (of gases or liquids) on rates of both hydrocracking (on metal-loaded zeolites) and catalytic cracking (on metal-free zeolites) has been well-documented. Sa-S9 Generally, C-C bond cleavage rates increase concomitantly with reactant chain lengths. The extraction of intrinsic cracking reaction rates, however, becomes progressively challenging with increasing reactant chain length (into the polymer regime), due to differences in accessible active (acid) sites, growing complexity of the reaction network (e.g., isomerization, hydrogen transfer, secondary  $\beta$ -scission, and deactivation), and interaction/ dynamics of the polymer melt with solid catalysts. These complications can significantly alter the residence times and inherent reactivities of reactants (or their cleaved fragments) within porous voids, which significantly affects measured reaction rates and product selectivities. Consequently, conversions are often reported in lieu of reaction rates to

facilitate reactivity comparisons for upcycling/conversion of bulky, long-chain molecules across different catalysts.

Though not as thorough as turnover numbers, solid conversion values serve as a helpful initial metric for comparisons of catalyst activity because they bypass the inherent challenges of obtaining intrinsic reaction rates for catalytic cracking of polymers and accurately measuring accessible active site densities (which vary with reaction time as smaller fragments access more active sites within microporous voids). In our prior study of polyethylene (PE) conversion under hydrogen using H-MFI zeolites, we estimated reaction rates by normalizing the mass of PE converted (i.e., solid conversion) by the total moles of Brønsted acid sites and reaction time (Figure 4). Our results

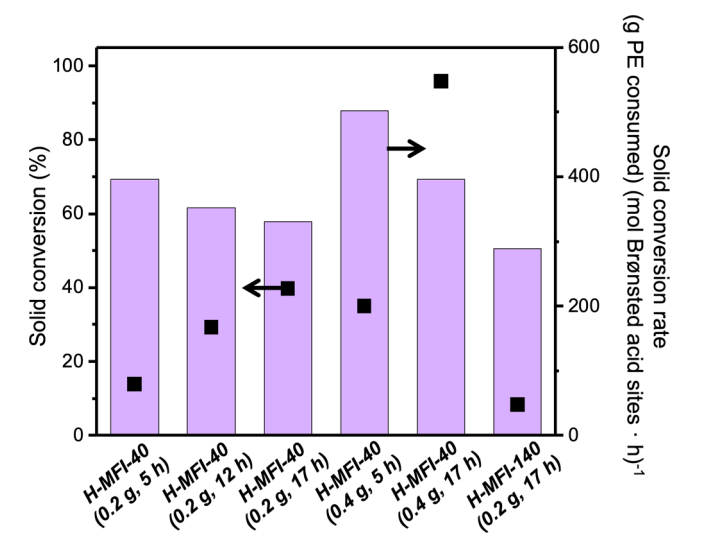


Figure 4. Solid conversion and solid conversion rates obtained from catalytic cracking of PE on H-MFI with different Si/Al ratios and catalyst loadings. Reaction condition: 473 K, 10 bar  $\rm H_2$ , 1 g of PE (Sigma-Aldrich, 4 kDa), 0.2–0.4 g of catalyst. Adapted from ref 60. Copyright 2023 Elsevier.

showed that solid conversion rates remained similar across MFI with different Si/Al and catalyst loadings, suggesting that our reaction rate estimates sufficiently compare performance of MFI zeolites with similar crystal sizes and framework structure when solid conversion is not at near-complete conversions. Although our solid conversion rates did not reflect actual (or intrinsic) reaction rates, since partial catalytic cracking of parent PE to lower molecular weight PE (still in solid form) and isomerization of parent PE chains are not considered, this rudimentary metric can still serve as a useful and reliable initial comparison as it only relies on the mass of solid residue extracted and the total density of active sites (i.e., Brønsted acid sites for catalytic cracking).

However, comparisons of solid conversion rates of PE (as defined above) are less accurate across zeolites of differing crystallite sizes or framework architectures, partially due to differences in densities of initially accessible protons. In contrast to catalytic cracking gaseous and short-chain liquid hydrocarbons, proton locations (internal micropores, surface, or mesopores if using hierarchical zeolites) bear important catalytic consequences on the catalytic cracking rates for bulky and long-chain molecules (i.e., plastics) that cannot directly access micropores within relevant time scales. For instance, thermogravimetric analysis (TGA) of a physical mixture of PE

and H-MFI titrated with 2,4,6-trimethylpyridine (PE + H-MFI-TMPy; held at 523 K for 5 h) in inert (Ar) gas flow showed a derivative weight loss comparable to that of pure PE (<0.04% min<sup>-1</sup>) but lower than that of PE + H-MFI (>0.10% min<sup>-1</sup>). Since the TMPy is too bulky to access the MFI channels (and thus only titrated surface protons), the similar derivative weight loss between PE + H-MFI-TMPy and pure PE suggested that bulky, polymeric molecules must first undergo activation and deconstruction on the surface protons of microporous zeolites, and only the smaller, cleaved fragments can access protons within microporous voids. Duan et al. similarly reported that PE decomposition on MFI nanosheets only gave trace conversions when coated with a thin layer of SiO<sub>2</sub>, which rendered surface protons inaccessible. <sup>61</sup>

For hierarchical zeolites, both the presence and accessibility of mesopores to the external zeolite surface need assessment. As stated before, mesopores can either be open (accessible to the external surface) or occluded (only accessible via micropores) (Figure 2). Kots et al. reported that HDPE deconstruction rates on Pt/Al<sub>2</sub>O<sub>3</sub> + H-MOR were six times higher with open mesopores (synthesized via dealumination and then desilication) than with occluded mesopores (synthesized via partial recrystallization), due to higher external surface area and proton accessibility with open mesopores.<sup>62</sup> This observation was consistent with the initial (accessible) surface protons being responsible for initial activation/cleavage and limited accessibility micropores to the parent PE chain, as the differences in conversion rates between H-MOR with open and occluded mesopores should be similar otherwise. In another study, it was proposed that the accessibility of zeolite micropores depends on the degree of polymer chain branching. 63 For instance, LLDPE  $(M_n =$ 48,190 Da; 16.6% branching) decomposition mainly occurs on the external surface of MFI, as solid conversion decreases from 91% to 16% when LLDPE is physically mixed with silicalitecoated MFI instead of uncoated MFI. Conversely, HDPE  $(M_n)$ = 20,263 Da; 0.7% branching) conversions were similar on coated and parent MFI, suggesting that the HDPE chains accessed more protons located within microporous voids.<sup>63</sup> Therefore, for PE with higher degree of branching, solid conversions normalized by surface Brønsted acid site densities (rather than bulk densities) are more accurate metrics to compare reactivities of catalysts differing in crystallite sizes or framework architecture. Thus, despite the importance of the microporous framework identity for product distribution (e.g., high selectivity to  $C_3-C_7$  gaseous products on MFI<sup>60,61,64,65</sup>), the initial activation of bulky polymers for both monofunctional catalytic cracking and bifunctional hydrocracking (with minimal hydrogenolysis) should depend on the quantity of surface or near-surface protons. Infrared spectroscopy, 66-69 solid state nuclear magnetic resonance spectroscopy, 66,67,70 and titration experiments<sup>71</sup> can all be utilized to quantify protons on the external surface of microporous and hierarchical zeolites.

Lastly, we highlight the possibility of using  $H_2$  to quantify catalytic turnovers for conversion of polyolefins in the presence of metal when the cleaved products are fully saturated, as during hydrocracking on bifunctional zeolites or hydrogenolysis on supported metals. This analysis infers that each C–C bond cleavage event will consume one molecule of  $H_2$ , since initial monomolecular activation or dehydrogenation of the parent alkane would produce one molecule of  $H_2$  before

undergoing  $\beta$ -scission, and the subsequent hydrogenation of the cleaved, unsaturated products would consume two molecules of  $H_2$ . When unsaturated hydrocarbons are present in the product distribution (e.g., for catalytic cracking of PE on metal-free zeolites), however, this method is not straightforward or appropriate as the correlation between C–C bond cleavage events and amount of  $H_2$  consumed becomes more vague.

### 5. HARNESSING DIFFUSION IN BIFUNCTIONAL CATALYSIS AND ITS IMPLICATIONS FOR REACTIVITY AND DEACTIVATION

Many of the same reaction-diffusion-deactivation architectures that describe Brønsted acid zeolites also apply to bifunctional catalytic systems, in which the additional function catalyzes a separate chemistry. This added chemistry influences catalysis at the acid sites by changing local concentrations of reactants, intermediates, and product species, ultimately enabling unique reactivities and selectivities not otherwise achieved by sequential processes of two independent functions.<sup>74</sup> Further, proximity of the additional sites to protons impacts this synergy because diffusion impacts the intracrystalline concentration gradients between functions. Proximity between sites has also been studied in tandem catalytic systems at the bed-scale, where the Peclet number is utilized to explain observed reactivity when participating functions exist at different axial positions along the catalyst bed.<sup>75</sup> While this is important to consider, it has been discussed elsewhere,<sup>24</sup> and this Viewpoint focuses on consequences of siting and diffusion on reaction and deactivation at shorter intracrystalline and intercrystalline length scales.

As metal sites can catalyze orthogonal chemistries to solid acids, their strategic coupling with acid catalysis can yield entirely different product pools compared to monofunctional acid catalysts. Remarkably, addition of metal functions (often as nanoparticles) to zeolites can increase catalyst lifetimes by scavenging coke precursors that would otherwise cause deactivation. We demonstrated this phenomenon in conversion of PE to short-chain hydrocarbons via metal-free and metal-loaded MFI.<sup>60</sup> Although proton-normalized solid conversion rates on MFI were greater than those on Pt- and Nisupported MFI, nearly no alkene products were observed for the latter due to rapid hydrogenation of alkenes on metal nanoparticles. The low gaseous alkene concentrations were likely also responsible for reduced solid conversion rates relative to metal-free MFI because alkenes readily undergo C-C bond cleavage ( $\beta$ -scission vs the alkane-cracking equivalent). Notably, however, higher catalyst lifetimes are expected for metal-loaded MFI than for metal-free MFI because rapid alkene hydrogenation mitigates formation of coke precursors. Indeed, differential thermogravimetric curves show accumulation of low molecular weight organics and absence of coke in spent Pt-MFI, whereas spent H-MFI contains significant portions of both foulants (Figure 5).

Moreover, we detected higher concentrations of aromatic products for metal-free MFI at shorter reaction times than Pt-loaded MFI. The prevention of coke formation may break down in the cases of significantly low metal to acid site ratio, high intracrystalline acid site density with solely external metal functions, or metals with lower hydrogenation reactivity than Pt, but our work highlights an example of how addition of metal functions to zeolites in the presence of hydrogen can be

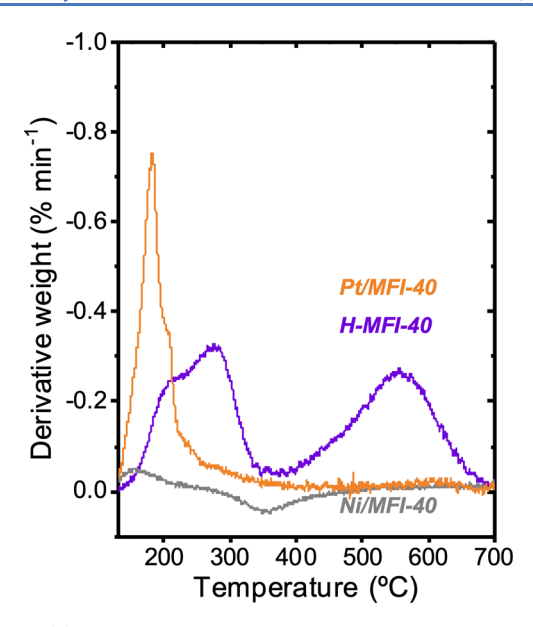


**Figure 5.** (a) Derivative weight curves of postreaction metal-loaded and metal-free MFI-40 after PE hydrocracking reactions (523 K, 10 bar H<sub>2</sub>, 17 h, 1 g of PE, and 0.2 g of catalyst; 100% solid conversion attained within reactor). Adapted from ref 60. Copyright 2023 Elsevier.

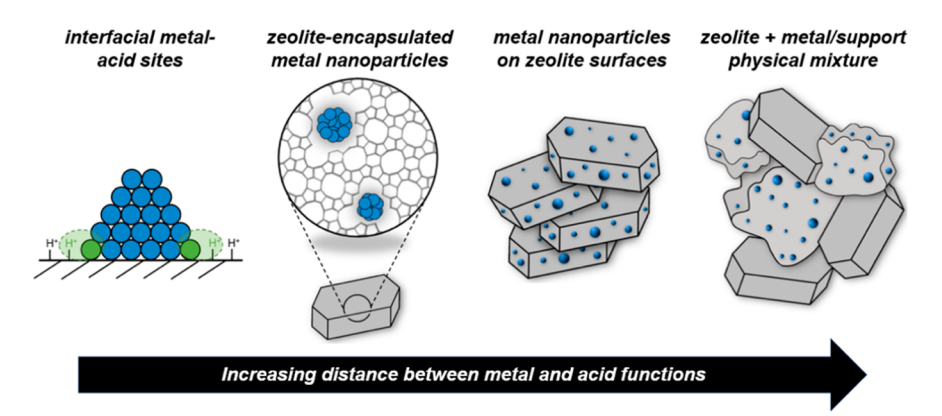
effective in preventing deactivation by coking versus metal-free equivalents. These extended catalyst lifetimes may be further enhanced by coupling this bifunctional catalysis with hierarchical zeolites, which retain higher reactivity than microporous zeolites at equivalent extents due to redistribution of coke deposits to mesopores.<sup>37</sup> The synergy between metals and mesopores was demonstrated during benzene alkylation by methanol, whereby the addition of Pt to MFI-h mitigated deactivation (via mesopores) and increased selectivity to toluene and xylene (via Pt-catalyzed hydrogenation of ethylene to prevent formation of ethylbenzene).<sup>76</sup> This study, combined with our observations in diffusion-limited hydrocarbon upgrading and PE conversion, demonstrates how metal functions may be leveraged alongside auxiliary mesoporosity to understand and mitigate coking.

The above example of bifunctional zeolites tested only one metal—acid proximity, namely metal nanoparticles supported on the external surface of zeolite (MFI) crystals. However, acid and metal functions can be separated at a variety of length

scales ranging from interfacial sites to physical mixtures depending on the material preparation (Scheme 1). Techniques such as incipient wetness impregnation and strong electrostatic adsorption with subsequent reduction are common methods to deposit metal nanoparticles on active supports. These methods often yield surface-supported metal nanoparticles, even for microporous zeolites and MOFs, hence rendering separate domains of metal catalysis on crystallite surfaces alongside intracrystalline acid catalysis. Though more synthetically challenging, metal nanoparticles can also be encapsulated within porous supports, not only increasing metal dispersions and thermal stability but also enabling unique reactivity relative to analogous surface-supported materials. 77-79 Notably, encapsulated metals benefit from diffusioncontrol imposed by the microporous supports to govern ingress and egress of chemical species according to their sizes. For example, Pd nanoparticles encapsulated in siliceous MFI were active for the hydrogenation of 3-methyl-2-butenal and cinnamaldehyde, while the turnover rate for the substituted 3,3-diphenylacrylaldehyde was negligible.<sup>80</sup> Reference Pd on the external surfaces of S-1 crystallites had similar reactivity for hydrogenation of all three enal reactants, suggesting that differences in rates observed for encapsulated Pd reflected the inability of the bulky aldehyde to access internal metal sites. This is analogous to observed reaction-diffusion during TMB alkylation with BA in MFI, wherein production of TM2B was solely catalyzed by external protons due to the inaccessibility of micropores to TMB.27

When confined in a catalytically active support, this diffusional control leveraged by encapsulated metals manifests in unique selectivities relative to surface-supported analogues. The siting of metal nanoparticles within zeolite frameworks dictates the order or frequency in which reactant molecules encounter various active sites as they diffuse from the bulk to the surface and through the micropores, as exemplified by the tandem aldol condensation and hydrogenation of furfural and acetone on Pt-MFI.81 When Pt is supported on the surface of MFI, furfural prematurely hydrogenates before diffusing into micropores, hence precluding the acid-catalyzed aldol condensation and promoting undesired side reactions such as decarbonylation. However, the MFI-encapsulated Pt catalyst gave 87% yield to desired C<sub>8</sub> products (compared to 24% by Pt on MFI) since siting Pt nanoparticles within MFI hindered furfural access to Pt, thus encouraging the acid-catalyzed aldol condensation to proceed prior to hydrogenation. Therefore,

Scheme 1. Bifunctional Zeolite-Metal Nanoparticle Catalysts Ordered as a Function of Increasing Distance between Functions



while introduction of a metal function to solid acid catalysts has been shown to facilitate enhanced selectivities and unique reactivities, it is critical to consider the consequences of metal location. Added active sites have important implications for diffusion, as it is diffusion to and from these functions as well as crosstalk between chemically distinct functions that often drives enhanced product distributions that are touted for tandem catalytic systems.

Proximity effects between functions are particularly notable in systems with severe diffusion limitations, as Thiele moduli for encapsulated metal functions are higher than those for surface-supported metals because slower molecular diffusion increases intracrystalline residence times. This was recently demonstrated for n-heptane isomerization on Pt-MFI, for which the presence of encapsulated Pt nanoparticles yielded higher observed isomerization rates than extracrystalline Pt. 82 Nanometer-scale Pt-proton proximities promote dehydrogenation of n-heptane and hydrogenation of isoalkenes that alleviate local equilibrium constraints, hence resulting in higher n-heptane turnover frequencies and selectivity to isoalkanes. These effects are felt more strongly for decreasing Pt-proton distances, as shown by a series of MFI-encapsulated Pt catalysts with varying fractions of encapsulated Pt in which enhancements of first-order rate constants for n-heptane isomerization relative to that of a physical mixture of Pt on silica with MFI increase with increasing degree of encapsulation. Similarly, metal-acid proximity effects are felt less strongly with decreasing internal diffusion limitation, since faster molecular diffusion is coupled with intrinsically lower isomerization and  $\beta$ -scission rates due to less effective confinement of transition states, ultimately yielding smaller Thiele moduli. Indeed, rate enhancement for Pt encapsulated in MFI relative to Pt and MFI physical mixtures is more drastic than that observed in analogous BEA materials. Similarly, no rate enhancement is observed for Pt in FAU. This study exemplifies the importance of leveraging (intersite) diffusion to control product distributions and increase turnover rates; however, proximity of chemically distinct sites is not always the key driver of reactivity.

In the case of interfacial sites, diffusion between functions does not play a role due to the bifunctional nature of the active site. For single-atom Pt on ceria, methanol dissociation, water dissociation, and the water gas shift reaction all occur in the proximity of the single-atom Pt active site in which Pt and O vacancies cooperatively perform these chemistries.<sup>83</sup> When diffusion between functions can play a role in the catalysis, its effects can be small relative to other dominating factors that influence intrinsic reactivity. In propylene epoxidation via Au/ Ti-oxide bifunctional catalysts, it is thought that Au generates hydrogen peroxide from molecular H2 and O2 while Ti centers catalyze propylene epoxidation via reactive hydrogen peroxidederived species. 84,85 Thus, shortening length scales of diffusion between Au and Ti functions is of interest to potentially increase the utilization efficiency of highly reactive peroxycontaining intermediates. Surprisingly, it was observed that Au encapsulated in titanium MFI (TS-1) was less active for propene epoxidation relative to surface-supported Au on TS-However, postsynthetic thermal treatments at temperatures required for removal of organic templates and ligands from TS-1-encapsulated Au resulted in elimination of particularly active subnanometer Au domains. This observation taken with the kinetic data suggests that close proximity of catalytic functions alone is insufficient in driving high

reactivity, since stronger factors such as intrinsic reactivity due to nanoparticle diameters may dominate.

#### 6. SUMMARY AND OUTLOOK

In this Viewpoint, we discussed the cooperativity and consequences of simultaneous reaction, diffusion, and deactivation in synthetically diverse zeolites containing chemically distinct active sites (acid or acid/metal) in different environments (micropores, mesopores, surfaces). Diffusion to or between these sites often impacts measured rates, selectivities, and stabilities of catalysts, hence rendering fundamental understanding of intrinsic active site properties difficult to assess and ultimately tune. This knowledge is vital to effectively and sustainably design next-generation catalysts that address growing demands for hard-to-decarbonize fuels and chemicals from closed-carbon (i.e.,  $\mathrm{CO}_2$  and waste plastic) and renewable (i.e., biomass) feedstocks.

We utilized four different examples to highlight how systematic studies can provide insight in the face of increasingly complex catalyst architectures and reaction pathways. First, gas-phase propene oligomerization illustrated how reactivity and selectivity change with zeolite pore size and pore connectivity, due to alterations of diffusivity as a function of reaction progress. The second example examined deactivation during parallel, liquid-phase alkylation and etherification reactions with kinetically relevant differences in diffusivity on a series of (hierarchical) zeolites with varying mesoporosity, crystal size, proton density, and micropore architecture. These two case studies used Thiele modulus (and effectiveness factor) formalisms to assess intrinsic kinetics based on measured parameters. The next reaction detailed further complications of hindered ingress of even larger molecules in the form of polyolefins, showing examples of rudimentary metrics that can be utilized to facilitate reactivity comparisons and the importance of accounting for accessibility in porous catalysts with pore sizes smaller than the reactants/ products. The final example extended these reactiondiffusion-deactivation phenomena to metal-acid zeolites where the proximity of the functions is vital to tune kinetics, selectivity, and deactivation, especially in diffusion-limited

The extensive advantages of hierarchical zeolites are thoroughly discussed in this Viewpoint. We argue that optimization of hierarchical zeolite catalysts requires better understanding of their underlying catalytic structure-function relationships, which depend on diffusion path lengths and morphologies, intracrystalline defect densities, and active site distributions. Additionally, it is desired to apply these materials to diffusionally hindered molecules, resulting in lower reactivities (due to significant concentration gradients), selectivities (due to diffusion-enhanced secondary reactions), or catalyst lifetimes (due to coke buildup in micropores). Such molecules include not only those discussed in this Viewpoint but also those involved in BTX formation from toluene disproportionation or methylation, biomass conversion to aviation fuel, and methane dehydroaromatization. Further, extraction of intrinsic kinetics is crucial for informed design of hierarchical and microporous zeolites (both metal-free or metal-loaded) for diffusion-limited transformations of platform molecules to fuels and chemicals. Through the systematic analyses of reaction-diffusion-deactivation illustrated in this Viewpoint, we demonstrate that proper treatment of limiting diffusion and deactivation does not completely limit kinetic insights. Therefore, effective reaction—diffusion—deactivation analysis will allow kinetics intuition to match rapid innovations in zeolite materials design.

#### AUTHOR INFORMATION

#### **Corresponding Author**

Michele L. Sarazen — Department of Chemical and Biological Engineering, Princeton University, Princeton, New Jersey 08544, United States; orcid.org/0000-0002-5732-7130; Email: msarazen@princeton.edu

#### **Authors**

Cole W. Hullfish — Department of Chemical and Biological Engineering, Princeton University, Princeton, New Jersey 08544, United States; orcid.org/0000-0001-6804-0517

Jun Zhi Tan — Department of Chemical and Biological Engineering, Princeton University, Princeton, New Jersey 08544, United States; orcid.org/0000-0002-9643-2232

Hayat I. Adawi — Department of Chemical and Biological Engineering, Princeton University, Princeton, New Jersey 08544, United States; orcid.org/0000-0002-7971-0739

Complete contact information is available at: https://pubs.acs.org/10.1021/acscatal.3c03559

#### **Author Contributions**

<sup>‡</sup>C.W.H., J.Z.T., and H.I.A. contributed to this work equally.

#### Notes

The authors declare no competing financial interest.

#### ACKNOWLEDGMENTS

This material is based upon work supported by the U.S. Department of Energy (DOE), Office of Science, Office of Basic Energy Sciences (BES), Division of Chemical Sciences, Geosciences and Biosciences through a subcontract from PNNL (FWP 78459), High Meadows Environmental Institute Grand Challenge Award at Princeton University, and the National Science Foundation (NSF-EFRI CBET-2029425). C.W.H. acknowledges partial support from the National Science Foundation Graduate Research Fellowship (NSF DGE-2039656).

#### REFERENCES

- (1) Zhao, H.; Ma, J.; Zhang, Q.; Liu, Z.; Li, R. Adsorption and Diffusion of N-Heptane and Toluene over Mesoporous ZSM-5 Zeolites. *Ind. Eng. Chem. Res.* **2014**, *53* (35), 13810–13819.
- (2) Galarneau, A.; Guenneau, F.; Gedeon, A.; Mereib, D.; Rodriguez, J.; Fajula, F.; Coasne, B. Probing Interconnectivity in Hierarchical Microporous/Mesoporous Materials Using Adsorption and Nuclear Magnetic Resonance Diffusion. *J. Phys. Chem. C* **2016**, 120 (3), 1562–1569.
- (3) Groen, J. C.; Zhu, W.; Brouwer, S.; Huynink, S. J.; Kapteijn, F.; Moulijn, J. A.; Pérez-Ramírez, J. Direct Demonstration of Enhanced Diffusion in Mesoporous ZSM-5 Zeolite Obtained via Controlled Desilication. *J. Am. Chem. Soc.* **2007**, *129* (2), 355–360.
- (4) Qin, Z.; Zeng, S.; Melinte, G.; Bučko, T.; Badawi, M.; Shen, Y.; Gilson, J.-P.; Ersen, O.; Wei, Y.; Liu, Z.; Liu, X.; Yan, Z.; Xu, S.; Valtchev, V.; Mintova, S. Understanding the Fundamentals of Microporosity Upgrading in Zeolites: Increasing Diffusion and Catalytic Performances. *Adv. Sci.* 2021, 8 (17), No. 2100001.
- (5) Bibby, D. M.; Milestone, N. B.; Patterson, J. E.; Aldridge, L. P. Coke Formation in Zeolite ZSM-5. *J. Catal.* **1986**, 97 (2), 493–502.
- (6) Bibby, D. M.; Howe, R. F.; McLellan, G. D. Coke Formation in High-Silica Zeolites. *Appl. Catal. A Gen.* **1992**, *93* (1), 1–34.

- (7) Bibby, D. M.; McLellan, G. D.; Howe, R. F. Effects of Coke Formation and Removal on the Acidity of ZSM-5. *Stud. Surf. Sci. Catal.* **1987**, *34*, 651–658.
- (8) Lee, K.; Lee, S.; Jun, Y.; Choi, M. Cooperative Effects of Zeolite Mesoporosity and Defect Sites on the Amount and Location of Coke Formation and Its Consequence in Deactivation. *J. Catal.* **2017**, *347*, 222–230
- (9) Olsbye, U.; Svelle, S.; Bjørgen, M.; Beato, P.; Janssens, T. V. W.; Joensen, F.; Bordiga, S.; Lillerud, K. P. Conversion of Methanol to Hydrocarbons: How Zeolite Cavity and Pore Size Controls Product Selectivity. *Angew. Chemie Int. Ed.* **2012**, *51* (24), 5810–5831.
- (10) Jun, Y.; Lee, S.; Lee, K.; Choi, M. Effects of Secondary Mesoporosity and Zeolite Crystallinity on Catalyst Deactivation of ZSM-5 in Propanal Conversion. *Microporous Mesoporous Mater.* **2017**, 245, 16–23.
- (11) Pines, H. 1-Acid-Catalyzed Reactions. In *The Chemistry of Catalytic Hydrocarbon Conversions*; Academic Press: Cambridge, MA, 1981; pp 1–122. DOI: 10.1016/B978-0-12-557160-9.50006-X.
- (12) Shephard, F. E.; Rooney, J. J.; Kemball, C. The Polymerization of Propylene on Silica-Alumina. *J. Catal.* **1962**, *1* (4), 379–388.
- (13) Biscardi, J. A.; Iglesia, E. Structure and Function of Metal Cations in Light Alkane Reactions Catalyzed by Modified H-ZSMS. *Catal. Today* **1996**, *31* (3), 207–231.
- (14) Mlinar, A. N.; Zimmerman, P. M.; Celik, F. E.; Head-Gordon, M.; Bell, A. T. Effects of Brønsted-Acid Site Proximity on the Oligomerization of Propene in H-MFI. *J. Catal.* **2012**, 288, 65–73.
- (15) Bandiera, J.; Taarit, Y. B. Elementary Reactions and Thermodynamic Effects in the Conversion of Propene over an Acidic A1MFI. *Appl. Catal. A Gen.* **1995**, *132* (1), 157–167.
- (16) Corma, A. Inorganic Solid Acids and Their Use in Acid-Catalyzed Hydrocarbon Reactions. *Chem. Rev.* **1995**, *95* (3), 559–614.
- (17) Gounder, R.; Iglesia, E. The Catalytic Diversity of Zeolites: Confinement and Solvation Effects within Voids of Molecular Dimensions. *Chem. Commun.* **2013**, 49 (34), 3491–3509.
- (18) Sarazen, M. L.; Doskocil, E.; Iglesia, E. Catalysis on Solid Acids: Mechanism and Catalyst Descriptors in Oligomerization Reactions of Light Alkenes. *J. Catal.* **2016**, 344, 553–569.
- (19) Sarazen, M. L.; Iglesia, E. Effects of Charge, Size, and Shape of Transition States, Bound Intermediates, and Confining Voids in Reactions of Alkenes on Solid Acids. *ChemCatChem.* **2018**, *10* (18), 4028–4037
- (20) Martens, J. A.; Verrelst, W. H.; Mathys, G. M.; Brown, S. H.; Jacobs, P. A. Tailored Catalytic Propene Trimerization over Acidic Zeolites with Tubular Pores. *Angew. Chemie Int. Ed.* **2005**, 44 (35), 5687–5690.
- (21) Sarazen, M. L.; Doskocil, E.; Iglesia, E. Effects of Void Environment and Acid Strength on Alkene Oligomerization Selectivity. ACS Catal. 2016, 6 (10), 7059–7070.
- (22) Bickel, E. E.; Lee, S.; Gounder, R. Influence of Brønsted Acid-Site Density on Reaction-Diffusion Phenomena That Govern Propene Oligomerization Rate and Selectivity in MFI Zeolites. *ACS Catal.* **2023**, *13* (2), 1257–1269.
- (23) Bickel, E. E.; Gounder, R. Hydrocarbon Products Occluded within Zeolite Micropores Impose Transport Barriers That Regulate Brønsted Acid-Catalyzed Propene Oligomerization. *JACS Au* **2022**, *2* (11), 2585–2595.
- (24) Noh, G.; Sarazen, M. L. Transport in Heterogeneous Catalysis Beyond Reactant Diffusion Limitations. *J. Catal.* **2021**, 404, 679–686.
- (25) Hartmann, M.; Machoke, A. G.; Schwieger, W. Catalytic Test Reactions for the Evaluation of Hierarchical Zeolites. *Chem. Soc. Rev.* **2016**, 45 (12), 3313–3330.
- (26) Peng, P.; Gao, X.-H.; Yan, Z.-F.; Mintova, S. Diffusion and Catalyst Efficiency in Hierarchical Zeolite Catalysts. *Natl. Sci. Rev.* **2020**, *7* (11), 1726–1742.
- (27) Adawi, H. I.; Odigie, F. O.; Sarazen, M. L. Alkylation of Poly-Substituted Aromatics to Probe Effects of Mesopores in Hierarchical

- Zeolites with Differing Frameworks and Crystal Sizes. *Mol. Syst. Des. Eng.* **2021**, *6* (11), 903–917.
- (28) Verboekend, D.; Pérez-Ramírez, J. Design of Hierarchical Zeolite Catalysts by Desilication. *Catal. Sci. Technol.* **2011**, *1* (6), 879–890.
- (29) Hu, H.; Ke, M.; Zhang, K.; Liu, Q.; Yu, P.; Liu, Y.; Li, C.; Liu, W. Designing Ferrierite-Based Catalysts with Improved Properties for Skeletal Isomerization of n-Butene to Isobutene. *RSC Adv.* **2017**, 7 (50), 31535–31543.
- (30) Almas, Q.; Sievers, C.; Jones, C. W. Role of the Mesopore Generation Method in Structure, Activity and Stability of MFI Catalysts in Glycerol Acetylation. *Appl. Catal. A Gen.* **2019**, *571*, 107–117
- (31) García-Martínez, J.; Johnson, M.; Valla, J.; Li, K.; Ying, J. Y. Mesostructured Zeolite Y—High Hydrothermal Stability and Superior FCC Catalytic Performance. *Catal. Sci. Technol.* **2012**, 2 (5), 987–994.
- (32) Li, X.; Prins, R.; van Bokhoven, J. A. Synthesis and Characterization of Mesoporous Mordenite. *J. Catal.* **2009**, 262 (2), 257–265.
- (33) Zhang, X.; Liu, D.; Xu, D.; Asahina, S.; Cychosz, K. A.; Agrawal, K. V.; Al Wahedi, Y.; Bhan, A.; Al Hashimi, S.; Terasaki, O.; Thommes, M.; Tsapatsis, M. Synthesis of Self-Pillared Zeolite Nanosheets by Repetitive Branching. *Science* (80-.). **2012**, 336 (6089), 1684–1687.
- (34) Xu, D.; Abdelrahman, O.; Ahn, S. H.; Guefrachi, Y.; Kuznetsov, A.; Ren, L.; Hwang, S.; Khaleel, M.; Al Hassan, S.; Liu, D.; Hong, S. B.; Dauenhauer, P.; Tsapatsis, M. A Quantitative Study of the Structure—Activity Relationship in Hierarchical Zeolites Using Liquid-Phase Reactions. *AIChE J.* **2019**, *65* (3), 1067–1075.
- (35) Tukur, N. M.; Al-Khattaf, S. Catalytic Transformation of 1,3,5-Trimethylbenzene over a USY Zeolite Catalyst. *Energy Fuels* **2007**, *21* (5), 2499–2508.
- (36) Gueudré, L.; Milina, M.; Mitchell, S.; Pérez-Ramírez, J. Superior Mass Transfer Properties of Technical Zeolite Bodies with Hierarchical Porosity. *Adv. Funct. Mater.* **2014**, 24 (2), 209–219.
- (37) Adawi, H. I.; Zheng, Y.; Sarazen, M. L. Underpinnings of Carbonaceous Deposition among Structurally Diverse Hierarchical Zeolites during Hydrocarbon Upgrading. *Cryst. Growth Des.* **2023**, 23 (4), 2675–2688.
- (38) Knaeble, W.; Iglesia, E. Acid Strength and Metal-Acid Proximity Effects on Methylcyclohexane Ring Contraction Turnover Rates and Selectivities. *J. Catal.* **2016**, 344, 817–830.
- (39) Noh, G.; Shi, Z.; Zones, S. I.; Iglesia, E. Isomerization and  $\beta$ -Scission Reactions of Alkanes on Bifunctional Metal-Acid Catalysts: Consequences of Confinement and Diffusional Constraints on Reactivity and Selectivity. *J. Catal.* **2018**, 368, 389–410.
- (40) DeLuca, M.; Hibbitts, D. Predicting Diffusion Barriers and Diffusivities of C6–C12 Methylbenzenes in MFI Zeolites. *Microporous Mesoporous Mater.* **2022**, 333, No. 111705.
- (41) Jobic, H.; Theodorou, D. N. Quasi-Elastic Neutron Scattering and Molecular Dynamics Simulation as Complementary Techniques for Studying Diffusion in Zeolites. *Microporous Mesoporous Mater.* **2007**, *102* (1), 21–50.
- (42) Smit, B.; Maesen, T. L. M. Molecular Simulations of Zeolites: Adsorption, Diffusion, and Shape Selectivity. *Chem. Rev.* **2008**, *108* (10), 4125–4184.
- (43) Karger, J.; Ruthven, D. M. On the Comparison between Macroscopic and n.m.r. Measurements of Intracrystalline Diffusion in Zeolites. *Zeolites* 1989, 9 (4), 267–281.
- (44) Davis, M. E.; Davis, R. J. Fundamentals of Chemical Reaction Engineering; McGraw-Hill Higher Education: New York, 2003.
- (45) Hwang, A.; Le, T. T.; Shi, Z.; Dai, H.; Rimer, J. D.; Bhan, A. Effects of Diffusional Constraints on Lifetime and Selectivity in Methanol-to-Olefins Catalysis on HSAPO-34. *J. Catal.* **2019**, 369, 122–132.
- (46) Kim, J.; Choi, M.; Ryoo, R. Effect of Mesoporosity against the Deactivation of MFI Zeolite Catalyst during the Methanol-to-Hydrocarbon Conversion Process. *J. Catal.* **2010**, 269 (1), 219–228.

- (47) Tzoulaki, D.; Jentys, A.; Pérez-Ramírez, J.; Egeblad, K.; Lercher, J. A. On the Location, Strength and Accessibility of Brønsted Acid Sites in Hierarchical ZSM-5 Particles. *Catal. Today* **2012**, *198* (1), 3–11.
- (48) Foley, B. L.; Johnson, B. A.; Bhan, A. A Method for Assessing Catalyst Deactivation: A Case Study on Methanol-to-Hydrocarbons Conversion. *ACS Catal.* **2019**, *9* (8), 7065–7072.
- (49) Fogler, S. H. Elements of Chemical Reaction Engineering, fifth ed.; Prentice Hall: Boston, MA, 2016.
- (50) Milina, M.; Mitchell, S.; Crivelli, P.; Cooke, D.; Pérez-Ramírez, J. Mesopore Quality Determines the Lifetime of Hierarchically Structured Zeolite Catalysts. *Nat. Commun.* **2014**, *5* (1), 3922.
- (51) Iadrat, P.; Horii, N.; Atithep, T.; Wattanakit, C. Effect of Pore Connectivity of Pore-Opened Hierarchical MOR Zeolites on Catalytic Behaviors and Coke Formation in Ethanol Dehydration. *ACS Appl. Mater. Interfaces* **2021**, *13* (7), 8294–8305.
- (52) Li, K.; Valla, J.; Garcia-Martinez, J. Realizing the Commercial Potential of Hierarchical Zeolites: New Opportunities in Catalytic Cracking. *ChemCatChem.* **2014**, *6* (1), 46–66.
- (53) Weitkamp, J. The Influence of Chain Length in Hydrocracking and Hydroisomerization of N-Alkanes. In *Hydrocracking and Hydrotreating*; ACS Symposium Series; American Chemical Society: Washington, DC, 1975; Vol. 20, p 1.
- (54) Abbot, J.; Dunstan, P. R. Catalytic Cracking of Linear Paraffins: Effects of Chain Length. *Ind. Eng. Chem. Res.* **1997**, 36 (1), 76–82.
- (55) Corma, A.; Miguel, P. J.; Orchille's, A. V. Influence of Hydrocarbon Chain Length and Zeolite Structure on the Catalyst Activity and Deactivation for N-Alkanes Cracking. *Appl. Catal. A Gen.* **1994**, *117* (1), 29–40.
- (56) Abbot, J.; Wojciechowski, B. W. Kinetics of Catalytic Cracking of N-Paraffins on HY Zeolite. *J. Catal.* 1987, 104 (1), 80–85.
- (57) Kissin, Y. V. Relative Reactivities of Alkanes in Catalytic Cracking Reactions. *J. Catal.* **1990**, *126* (2), 600–609.
- (58) Kissin, Y. V. Relative Reactivities of Alkanes in Multi-Component Catalytic Cracking Reactions. *Catal. Lett.* **1993**, *19* (2), 181–187.
- (59) Nace, D. M. Catalytic Cracking over Crystalline Aluminosilicates. I. Instantaneous Rate Measurements for Hexadecane Cracking. *Prod. R&D* **1969**, *8* (1), 24–31.
- (60) Tan, J. Z.; Hullfish, C. W.; Zheng, Y.; Koel, B. E.; Sarazen, M. L. Conversion of Polyethylene Waste to Short Chain Hydrocarbons under Mild Temperature and Hydrogen Pressure with Metal-Free and Metal-Loaded MFI Zeolites. *Appl. Catal. B Environ.* **2023**, 338, No. 123028.
- (61) Duan, J.; Chen, W.; Wang, C.; Wang, L.; Liu, Z.; Yi, X.; Fang, W.; Wang, H.; Wei, H.; Xu, S.; Yang, Y.; Yang, Q.; Bao, Z.; Zhang, Z.; Ren, Q.; Zhou, H.; Qin, X.; Zheng, A.; Xiao, F.-S. Coking-Resistant Polyethylene Upcycling Modulated by Zeolite Micropore Diffusion. J. Am. Chem. Soc. 2022, 144 (31), 14269–14277.
- (62) Kots, P. A.; Doika, P. A.; Vance, B. C.; Najmi, S.; Vlachos, D. G. Tuning High-Density Polyethylene Hydrocracking through Mordenite Zeolite Crystal Engineering. *ACS Sustain. Chem. Eng.* **2023**, *11* (24), 9000–9009.
- (63) Jerdy, A. C.; Trevisi, L.; Monwar, M.; González-Borja, M. Á.; Abbott, R.; Lobban, L.; Crossley, S. Deconvoluting the Roles of Polyolefin Branching and Unsaturation on Depolymerization Reactions over Acid Catalysts. *Appl. Catal. B Environ.* **2023**, 337, No. 122986.
- (64) Zichittella, G.; Ebrahim, A. M.; Zhu, J.; Brenner, A. E.; Drake, G.; Beckham, G. T.; Bare, S. R.; Rorrer, J. E.; Román-Leshkov, Y. Hydrogenolysis of Polyethylene and Polypropylene into Propane over Cobalt-Based Catalysts. *JACS Au* **2022**, *2* (10), 2259–2268.
- (65) Liu, S.; Kots, P. A.; Vance, B. C.; Danielson, A.; Vlachos, D. G. Plastic Waste to Fuels by Hydrocracking at Mild Conditions. *Sci. Adv.* **2021**, *7* (17), No. eabf8283.
- (66) Freitas, C.; Barrow, N.; Zholobenko, V. Accessibility and Location of Acid Sites in Zeolites as Probed by FTIR and MAS-NMR. *Johnson Matthey Technol. Rev.* **2018**, 62, 279.

- (67) Paul, G.; Bisio, C.; Braschi, I.; Cossi, M.; Gatti, G.; Gianotti, E.; Marchese, L. Combined Solid-State NMR, FT-IR and Computational Studies on Layered and Porous Materials. *Chem. Soc. Rev.* **2018**, 47 (15), 5684–5739.
- (68) Thibault-Starzyk, F.; Stan, I.; Abelló, S.; Bonilla, A.; Thomas, K.; Fernandez, C.; Gilson, J. P.; Pérez-Ramírez, J. Quantification of Enhanced Acid Site Accessibility in Hierarchical Zeolites The Accessibility Index. *J. Catal.* **2009**, *264* (1), 11–14.
- (69) Beutel, T. W.; Willard, A. M.; Lee, C.; Martinez, M. S.; Dugan, R. Probing External Brønsted Acid Sites in Large Pore Zeolites with Infrared Spectroscopy of Adsorbed 2,4,6-Tri-Tert-Butylpyridine. *J. Phys. Chem. C* 2021, 125 (16), 8518–8532.
- (70) Yang, W.; Wang, Z.; Huang, J.; Jiang, Y. Qualitative and Quantitative Analysis of Acid Properties for Solid Acids by Solid-State Nuclear Magnetic Resonance Spectroscopy. *J. Phys. Chem. C* **2021**, 125 (19), 10179–10197.
- (71) Wu, Y.; Emdadi, L.; Qin, D.; Zhang, J.; Liu, D. Quantification of External Surface and Pore Mouth Acid Sites in Unit-Cell Thick Pillared MFI and Pillared MWW Zeolites. *Microporous Mesoporous Mater.* **2017**, 241, 43–51.
- (72) Hancock, J. N.; Rorrer, J. E. Hydrogen-Free Catalytic Depolymerization of Waste Polyolefins at Mild Temperatures. *Appl. Catal. B Environ.* **2023**, 338, No. 123071.
- (73) Rorrer, J. E.; Ebrahim, A. M.; Questell-Santiago, Y.; Zhu, J.; Troyano-Valls, C.; Asundi, A. S.; Brenner, A. E.; Bare, S. R.; Tassone, C. J.; Beckham, G. T.; Román-Leshkov, Y. Role of Bifunctional Ru/Acid Catalysts in the Selective Hydrocracking of Polyethylene and Polypropylene Waste to Liquid Hydrocarbons. *ACS Catal.* **2022**, *12*, 13969–13979.
- (74) Climent, M. J.; Corma, A.; Iborra, S.; Sabater, M. J. Heterogeneous Catalysis for Tandem Reactions. *ACS Catal.* **2014**, *4* (3), 870–891.
- (75) Razdan, N. K.; Kumar, A.; Bhan, A. Controlling Kinetic and Diffusive Length-Scales during Absorptive Hydrogen Removal in Methane Dehydroaromatization on MoCx/H-ZSM-5 Catalysts. *J. Catal.* **2019**, 372, 370–381.
- (76) Hu, H.; Zhang, Q.; Cen, J.; Li, X. Catalytic Activity of Pt Modified Hierarchical ZSM-5 Catalysts in Benzene Alkylation with Methanol. *Catal. Lett.* **2015**, *145* (2), *715–722*.
- (77) Otto, T.; Ramallo-López, J. M.; Giovanetti, L. J.; Requejo, F. G.; Zones, S. I.; Iglesia, E. Synthesis of Stable Monodisperse AuPd, AuPt, and PdPt Bimetallic Clusters Encapsulated within LTA-Zeolites. J. Catal. 2016, 342, 125–137.
- (78) Liu, J.-Y.; Chen, J.-F.; Zhang, Y. Cobalt-Imbedded Zeolite Catalyst for Direct Syntheses of Gasoline via Fischer—Tropsch Synthesis. *Catal. Sci. Technol.* **2013**, 3 (10), 2559–2564.
- (79) He, J.; Wu, Z.; Gu, Q.; Liu, Y.; Chu, S.; Chen, S.; Zhang, Y.; Yang, B.; Chen, T.; Wang, A.; Weckhuysen, B. M.; Zhang, T.; Luo, W. Zeolite-Tailored Active Site Proximity for the Efficient Production of Pentanoic Biofuels. *Angew. Chemie Int. Ed.* **2021**, *60* (44), 23713–23721.
- (80) Liu, C.; Liu, J.; Yang, S.; Cao, C.; Song, W. Palladium Nanoparticles Encapsulated in a Silicalite-1 Zeolite Shell for Size-Selective Catalysis in Liquid-Phase Solution. *ChemCatChem.* **2016**, 8 (7), 1279–1282.
- (81) Cho, H. J.; Kim, D.; Li, J.; Su, D.; Xu, B. Zeolite-Encapsulated Pt Nanoparticles for Tandem Catalysis. *J. Am. Chem. Soc.* **2018**, *140* (41), 13514–13520.
- (82) Hu, W.; Noh, G.; Iglesia, E. Consequences of Metal-Acid Site Proximity for Alkane Isomerization and  $\beta$ -Scission Mediated by Bifunctional Catalytic Cascades. *J. Catal.* **2023**, 425, 125–142.
- (83) Chen, L.; Qi, Z.; Peng, X.; Chen, J.-L.; Pao, C.-W.; Zhang, X.; Dun, C.; Young, M.; Prendergast, D.; Urban, J. J.; Guo, J.; Somorjai, G. A.; Su, J. Insights into the Mechanism of Methanol Steam Reforming Tandem Reaction over CeO2 Supported Single-Site Catalysts. J. Am. Chem. Soc. 2021, 143 (31), 12074–12081.
- (84) Kanungo, S.; Perez Ferrandez, D. M.; Neira d'Angelo, F.; Schouten, J. C.; Nijhuis, T. A. Kinetic Study of Propene Oxide and

- Water Formation in Hydro-Epoxidation of Propene on Au/Ti-SiO2 Catalyst. *J. Catal.* **2016**, 338, 284-294.
- (85) Hutchings, G. J. Nanocrystalline Gold and Gold Palladium Alloy Catalysts for Chemical Synthesis. *Chem. Commun.* **2008**, *10*, 1148–1164.
- (86) Otto, T.; Zhou, X.; Zones, S. I.; Iglesia, E. Synthesis, Characterization, and Function of Au Nanoparticles within TS-1 Zeotypes as Catalysts for Alkene Epoxidation Using O2/H2O Reactants. *J. Catal.* **2022**, *410*, 206–220.